PCCP

ROYAL SOCIETY OF CHEMISTRY

PAPER

Cite this: *Phys. Chem. Chem. Phys.*, 2020, **22**, 7440

Redox-active polyamine-salt aggregates as multistimuli-responsive soft nanoparticles†

Santiago E. Herrera, [a] Maximiliano L. Agazzi, [a] M. Lorena Cortez, [a] Waldemar A. Marmisollé, [a] Mario Tagliazucchi [b] and Omar Azzaroni *[a]

Received 6th January 2020,
Accepted 13th March 2020

DOI: 10.1039/d0cp00077a

rsc.li/pccp

Polyamine-salt aggregates have become promising soft materials in nanotechnology due to their easy preparation process and pH-responsiveness. Here, we report the use of hexacyanoferrate(II) and hexacyanoferrate(III) as electroactive crosslinking agents for the formation of nanometer-sized redox-active polyamine-redox-salt aggregates (rPSA) in bulk suspension. This nanoplatform can be selectively assembled or disassembled under different stimuli such as redox environment, pH and ionic strength. By changing the charge of the building blocks, external triggers allow switching the system between two phase states: aggregate-free solution or colloidal rPSA dispersion. The stimuli-activated modulation of the assembly/disassembly processes opens a path to exploit rPSA in technologies based on smart nanomaterials.

Introduction

Soft-matter devices and materials with responses to stimuli such as temperature, pH, ionic strength, redox-active species and light have rapidly gained importance in materials science and nanotechnology.[1–3] In this sense, the combination of different types of responsiveness in a single system led to the generation of multistimuli-responsive materials.[4,5] Thus, different multistimuli-responsive systems have been designed such as polymers, microgels, micelles, vesicles, and films.[6–11] Overall, these platforms are based on the integration of distinct functional units, which requires complex and expensive synthetic routes.

In this scenario, bioinspired polyamine-salt aggregates (PSA) based on electrostatically-driven self-assembly of polyamines have been widely studied due to their simple preparation methods, high loading efficiencies and stimuli-responsive capability.[12] In this approach, multivalent anions are used as ionic crosslinkers to form the supramolecular network.[13–16] As this network is mainly stabilized by electrostatic interactions, PSA are able to respond to stimuli that alter the charge of their building blocks. Thus, the use of anionic crosslinkers with switchable charge in the presence of external triggers allows the stimuli-driven modulation of the assembly/disassembly processes. For instance, the use of phosphate anions leads to the generation of PSA that can be disassembled in acidic environments by protonation of phosphate groups.[17–19] In another approach, the light and redox sensitivities of the ferrioxalate anion have been exploited to produce multi-stimuli responsive PSA.[20] In that system, UV irradiation or the action of a reducing agent decreases the charge of the anion and consequently leads to the disassembly of the PSA.

Other kinds of multivalent anions that present redox-tunable charge and switchable interactions with polyelectrolytes are hexacyanoferrates, such as trivalent ferricyanide ($[Fe(CN)_6]^{3-}$) and tetravalent ferrocyanide ($[Fe(CN)_6]^{4-}$). The complexation of strong polyelectrolytes with hexacyanoferrate anions has been explored in several studies.[21–29] These reports showed that the interaction is strongest with the less charged anion $[Fe(CN)_6]^{3-}$ compared to $[Fe(CN)_6]^{4-}$ due to ion-specific effects.[27] These differences have been even exploited for the formation of electroactive films by electrochemical deposition.[30–32] Thus, the anodic oxidation of $[Fe(CN)_6]^{4-}$ converts a soluble $[Fe(CN)_6]^{4-}$/polymer molecular complex to an insoluble $[Fe(CN)_6]^{3-}$/polymer aggregate that is deposited on the electrode surface. On the other hand, Plamper *et al.* applied these principles for activating the reversible aggregation of unimeric polymers to micellar aggregates using quaternized miktoarm star polymers as building blocks.[33] Following a similar approach, the size modulation of a thermo-responsive microgel has been recently demonstrated by electrochemically changing the charge of hexacyanoferrate anions trapped in the crosslinked network.[34]

Here we introduce the use of hexacyanoferrate anions as electroactive crosslinkers to generate redox-active polyamine-salt

[a] *Instituto de Investigaciones Fisicoquímicas Teóricas y Aplicadas (INIFTA), departamento de Química, Facultad de Ciencias Exactas, Universidad Nacional de La Plata – CONICET, Sucursal 4, Casilla de Correo 16, 1900 La Plata, Argentina. E-mail: azzaroni@inifta.unlp.edu.ar; Web: http://softmatter.quimica.unlp.edu.ar, www.twitter.com/softmatterlab, www.facebook.com/SoftMatterLaboratory*

[b] *Departamento de Química Inorgánica, Analítica y Química Física, INQUIMAE-CONICET, Facultad de Ciencias Exactas y Naturales, Ciudad Universitaria, Pabellón 2, Buenos Aires C1428EHA, Argentina*

† Electronic supplementary information (ESI) available. See DOI: 10.1039/d0cp00077a

aggregates (rPSA). We use commercial polyethylenimine (PEI) – a weak polycation that consists of a mixture of primary, secondary, and tertiary amine groups – as a polymeric building block. Weak polyelectrolytes also present dissimilar interactions with hexacyanoferrate anions. However, unlike strong polycations, they complex more strongly with the more charged $[Fe(CN)_6]^{4-}$ anion.[35–38] We explore the rPSA formation by varying the molar ratio between PEI and hexacyanoferrates(II,III) in different experimental conditions of pH and ionic strength. This exploration was performed in order to determine the regions where PSA are formed and those where there are no aggregates. Then, we show how the assembly/disassembly processes of rPSA can be rationally activated in response to different stimuli, including pH and ionic strength changes and the presence of redox agents. The multi-responsive character found for rPSA makes these smart systems promising candidates for advanced material engineering.

Materials and methods

Materials

Polyethylenimine (PEI, branched, M_w = 10 000 and 750 000) was purchased from Polysciences. Potassium hexacyanoferrate(II) trihydrate, potassium hexacyanoferrate(III), sodium chloride (NaCl), L-ascorbic acid, potassium permanganate ($KMnO_4$), poly(diallyldimethylammonium chloride) solution (PDDA, 20 wt% in H_2O, M_w = 100 000–200 000) and Trizma base were purchased from Sigma-Aldrich. Sodium hydroxide, hydrochloric acid and glacial acetic acid were purchased from Anedra. All chemicals were used without further purification.

Redox-active polyamine-salt aggregate (rPSA) formation

All rPSA colloidal dispersions were prepared by mixing different volumes of stock solutions of PEI (M_w = 10 000, 50 mM monomer concentration), $K_4Fe(CN)_6$ (25 mM), and $K_3Fe(CN)_6$ (25 mM), and completing the final concentration with buffer solution. Except for pH-triggered rPSA disassembly experiments (Fig. 4a and Fig. S7, ESI†), all solutions were prepared by using either 0.2 M acetate buffer at pH 3.5 or 0.2 M tris buffer at pH 9 (aqueous solutions). The mixing of reagents was conducted under vigorous stirring. The reagents were added in the following order: (1) PEI, (2) buffer, and (3) crosslinker.

rPSA phase diagram construction

Phase diagrams without added salt were constructed using aqueous stock solutions of polyamine and crosslinker in 0.2 M acetate buffer (pH 3.5) and 0.2 M tris buffer (pH 9). Phase diagrams with added salt were constructed using aqueous stock solutions of polyamine and crosslinker in 0.2 M acetate buffer (pH 3.5) containing 0.2 M NaCl. Briefly, 5 mL of polyamine solution (10 kDa PEI, 750 kDa PEI or 100–200 kDa PDDA) with a concentration of 1 mM monomer was placed in a 10 mL beaker containing a small magnetic bar. Next, a small volume (10 μL) of a 25 mM crosslinker solution was added into the beaker under continuous magnetic stirring. The addition of crosslinker was repeated until stable turbidity was detected. The final concentrations of polyamine and crosslinker were calculated by applying dilution factors. The procedure was repeated for different polyamine concentrations between 1 and 30 mM to construct the phase diagram.

pH, ionic strength, and redox response experiments

For the pH-triggered rPSA assembly/disassembly experiments, 2 mL of a mixture of 20 mM PEI and 2 mM crosslinker ($K_4Fe(CN)_6$ or $K_3Fe(CN)_6$) was placed in a plastic cuvette. In this case, all solutions were prepared using water instead of buffer solutions. Next, different amounts of concentrated NaOH and HCl were added, scanning the pH between 3.5 and 9 while registering the transmittance at λ = 580 nm with a spectrophotometer. For the experiment where rPSA disassembly was triggered by changes in ionic strength, 2 mL of a mixture of 20 mM PEI and 3 mM $K_3Fe(CN)_6$ at pH 3.5 (acetate buffer, without added salt) was placed in a plastic cuvette. Next, different amounts of concentrated NaCl were added while registering the transmittance at λ = 580 nm. For the redox-triggered rPSA assembly/disassembly experiments, 2 mL of a mixture of 15 mM PEI and 1.5 mM crosslinker ($K_4Fe(CN)_6$ or $K_3Fe(CN)_6$) at pH 3.5 (acetate buffer, without added salt) was placed in a plastic cuvette inside the spectrophotometer. A kinetic measurement at λ = 580 nm was started. After registering a stable transmittance signal, the cuvette was removed and 10 μL of oxidizing (0.1 M $KMnO_4$) or reducing (0.25 M ascorbic acid) agent was quickly added and vigorously stirred, and the cuvette was placed back into the spectrophotometer in order to follow the changes in transmittance due to the assembly/disassembly of Fe(II/III)-rPSA.

Dynamic light scattering (DLS) and ζ-potential measurements

DLS measurements were carried out with a ZetaSizer Nano (ZEN3600, Malvern, U.K.) using a quartz cuvette with a screw cap to prevent contamination with molecular oxygen. All measurements were made using a 173° backscatter angle with 10 runs (20 s run^{-1}), a fixed sensor position (1.25 mm), and non-fixed filter attenuation. ζ-Potential measurements were carried out using DTS1060 disposable cuvettes. The particle ζ-potential was obtained from the electrophoretic mobility with laser doppler velocimetry using a general-purpose analysis model in a 100 run experiment. The temperature was set to 20 °C in all measurements.

Atomic force microscopy (AFM) measurements

AFM measurements (Keysight N9418S 9500 AFM/SPM) were carried out in contact mode using a triangular silicon tip PointProbe® Plus (PPP-CONT, Nanosensors) with a typical force constant of 0.2 N m^{-1}. A drop of an Fe(II)-rPSA or Fe(III)-rPSA sample (1 mM PEI, 0.198 mM $[Fe(CN)_6]^{4-}$ or 0.198 mM $[Fe(CN)_6]^{3-}$ at pH 3.5 in acetate buffer without added salt) was placed over a clean highly oriented pyrolytic graphite (HOPG) substrate. After 2 minutes of PSA adsorption, the liquid drop was removed and the substrate was dried under a stream of nitrogen. Image analysis was performed with Gwyddion 2.5 software (http://gwyddion.net/).

UV-vis spectroscopy measurements

UV-vis experiments were carried out using a PerkinElmer Lambda 35 spectrometer. All rPSA spectra were measured between 700 and 350 nm using a quartz cuvette with a screw cap (5 mL, 1 cm path length) at 20 °C. Kinetics, pH and ionic strength response measurements were conducted at λ = 580 nm using a closed plastic cuvette (5 mL, 1 cm path length) at 20 °C.

Results and discussion

It has been previously demonstrated that the main driving force to produce the condensation of polyamine chains that leads to polyamine-salt aggregates (PSA) is the electrostatic interaction between the protonated polymer amine groups and the negatively charged crosslinkers.[39] In this way, regardless of the nature of the polyamine, different crosslinkers can be used in PSA preparation such as phosphate, pyrophosphate, tripolyphosphate, citrate, metal complexes and biomolecules.[12,14,20] There are several variables that control the formation and stability of PSA. In this sense, the formation and, eventually, the dissolution of PSA can be achieved by controlling the state of charge of both the polyamine and the crosslinker. Therefore, when the polyamine presents acid/base chemistry, the pH plays a crucial role as the charge of the polyamine can be externally regulated.[40] This is the case of polyamines that contains primary, secondary and tertiary amine groups in their structure. On the other hand, the formation and dissolution of PSA can also be regulated by altering the negative charge of the crosslinker. While increasing the charge of the crosslinker enhances the formation of PSA, a decrease in the charge leads to destabilization of the PSA supramolecular matrix. Different strategies to modulate the charge of the crosslinker have been exploited. For example, when a crosslinker presents an acid/base equilibrium, the charge can be pH-regulated.[19] On the other hand, when a redox-active complex is employed, the addition of a reducing or oxidizing agent can alter the charge of the crosslinker.[20]

In this work we study the crosslinking of polyethylenimine (PEI) with the electroactive anions hexacyanoferrate(II) ($[Fe(CN)_6]^{4-}$) and hexacyanoferrate(III) ($[Fe(CN)_6]^{3-}$), with the aim of building redox-active polyamine-salt aggregates (rPSA) able to respond to multiple stimuli (Scheme 1). Different variables such as concentration, pH, ionic strength and redox environment are investigated for controlling the formation and dissolution of rPSA.

rPSA preparation and characterization

The synthesis of PSA is characterized by its easiness and quickness in comparison with the synthesis of other soft functional materials such as microgels, which involves complex and expensive organic synthetic routes.[41,42] Scheme 1 presents the formation of a rPSA by direct mixing of aqueous solutions of PEI and crosslinkers ($[Fe(CN)_6]^{4-}$ or $[Fe(CN)_6]^{3-}$). Usually, the complexation between the polyamine and the crosslinker leads to pH changes in the solution due to a shift in the apparent pK_a of the polyamine.[19] Therefore, to fix the protonation of PEI we carried out the rPSA synthesis in 0.2 M acetate buffer at pH 3.5 or 0.2 M tris buffer at pH 9.

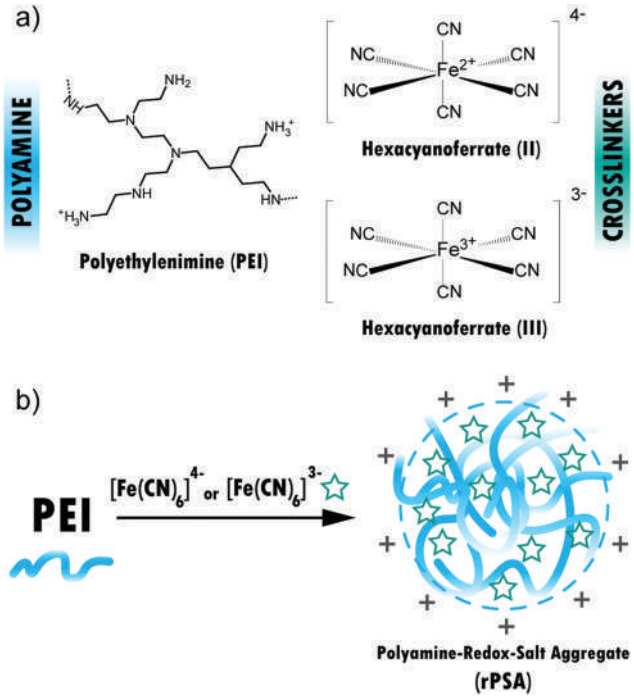

Scheme 1 Chemical structures of PEI, $[Fe(CN)_6]^{4-}$ and $[Fe(CN)_6]^{3-}$ (a) and the formation of a rPSA by crosslinking of PEI chains (b).

For the initial characterization of the $[Fe(CN)_6]^{4-}$-based rPSA (Fe(II)-rPSA) and the $[Fe(CN)_6]^{3-}$-based rPSA (Fe(III)-rPSA), the concentration of PEI was set to 1 mM (monomer concentration) and the crosslinker concentration was set to the minimum required to produce phase condensation (0.198 mM). Under this condition (PEI excess), the rPSA presents a maximum ζ-potential, guaranteeing optimal colloidal stability. We characterized the Fe(II)- and Fe(III)-based colloidal dispersions by dynamic light scattering (DLS), varying the pH (3.5 and 9), with and without added salt (NaCl 0.2 M). Table 1 presents the measurement results for the different rPSA under study. DLS size distribution plots are shown in Fig. S1 (ESI†).

Table 1 DLS characterization of rPSA colloidal dispersions prepared at different pH and ionic strength. The PEI concentration was set to 1 mM in all samples

rPSA	Crosslinker concentration (mM)	pH	NaCl 0.2 M	d (nm)	PDI	ζ (mV)
PEI-Fe(II)	0.198	3.5	No	134	0.159	+33
PEI-Fe(III)	0.198	3.5	No	233	0.104	+20.7
PEI-Fe(II)	0.149	3.5	Yes	Not stable	—	+21.7
PEI-Fe(III)	2.273	3.5	Yes	Not stable	—	+11.5
PEI-Fe(II)	0.149	9.0	No	215	0.176	+8.7
PEI-Fe(III)	0.247	9.0	No	280	0.201	+9.5

d, PDI and ζ correspond to the mean hydrodynamic diameter, polydispersity index and ζ-potential, respectively.

While PSA formation is driven by electrostatic attractions between a polyamine and multivalent anions (counterion condensation), the aggregate growth mechanism can be understood by considering a dynamic balance of electrostatic repulsion and van der Waals attraction between polyamine-salt complexes. These aggregates grow as a function of time by coalescence, and the growth rates depend on their surface charge.[39] In this sense, particles with less charged surfaces are more susceptible to aggregation (a higher growth rate of PSA) since the van der Waals attractive energy between the aggregates overcomes the repulsive energy of the charged surfaces. In contrast, particles with high surface charge will have lower growth rates due to the preponderance of repulsive interactions between aggregates.

For our systems without added salt it can be observed that, independently of the pH, the hydrodynamic diameters of the Fe(III)-rPSA are larger than those of the Fe(II)-rPSA. At pH 3.5, the smallest size observed for the Fe(II)-rPSA is consistent with its highest ζ-potential value. Analyzing the systems without added salt at different pH, it can be seen that when the pH is raised from 3.5 to 9 there is an increase in the size and a decrease in the ζ-potential of both the Fe(III)- and Fe(II)-rPSA due to deprotonation of PEI amine groups. In this way, the repulsion among the aggregates decreases and the PSA growth rate by coalescence increases.

The addition of salt into the system produces three major consequences: (1) a notable increase in the minimum $[Fe(CN)_6]^{3-}$ concentration to produce phase condensation, (2) a lowering of the ζ-potential, and (3) the destabilization of colloidal dispersions as the sizes tend to increase over time. The addition of salt produces the screening of the rPSA surface charges, giving, as a result, a slow aggregation of colloids. Also, the screening of amine charges in PEI has an impact on the minimum $[Fe(CN)_6]^{3-}$ concentration to produce Fe(III)-rPSA formation. Interestingly, this behavior was not observed for the case of the Fe(II)-rPSA system, as we further discuss in the next section.

We further characterized the rPSA colloids by AFM. Fig. 1 shows AFM topography images of Fe(II)-rPSA (Fig. 1a) and Fe(III)-rPSA (Fig. 1b) prepared at pH 3.5 adsorbed on top of highly oriented pyrolytic graphite (HOPG). The images show a homogeneous distribution of particles with an average diameter of 200 nm for Fe(II)-rPSA and 250 nm for Fe(III)-rPSA, and a height that varies between 15 and 120 nm. The fact that the diameter and height of the particles do not coincide can be explained in terms of a partial deformation that takes place when a spherical soft colloid comes into contact with the surface of a substrate.[43–47] This behavior was previously observed during the construction of layer-by-layer films using PSA as positive building blocks on glass slides.[48] In this context, the ratio between the height and diameter can be attributed to the degree of deformation, where 1 corresponds to a perfect sphere and 0 corresponds to a completely deformed particle (plane). Fig. 1c shows a linear correlation between the height and diameter for both the Fe(II)- and Fe(III)-rPSA with slopes of 0.09 and 0.4, respectively. Thus, the Fe(II)-rPSA present less deformation (60%) than the Fe(III)-rPSA (90%) in

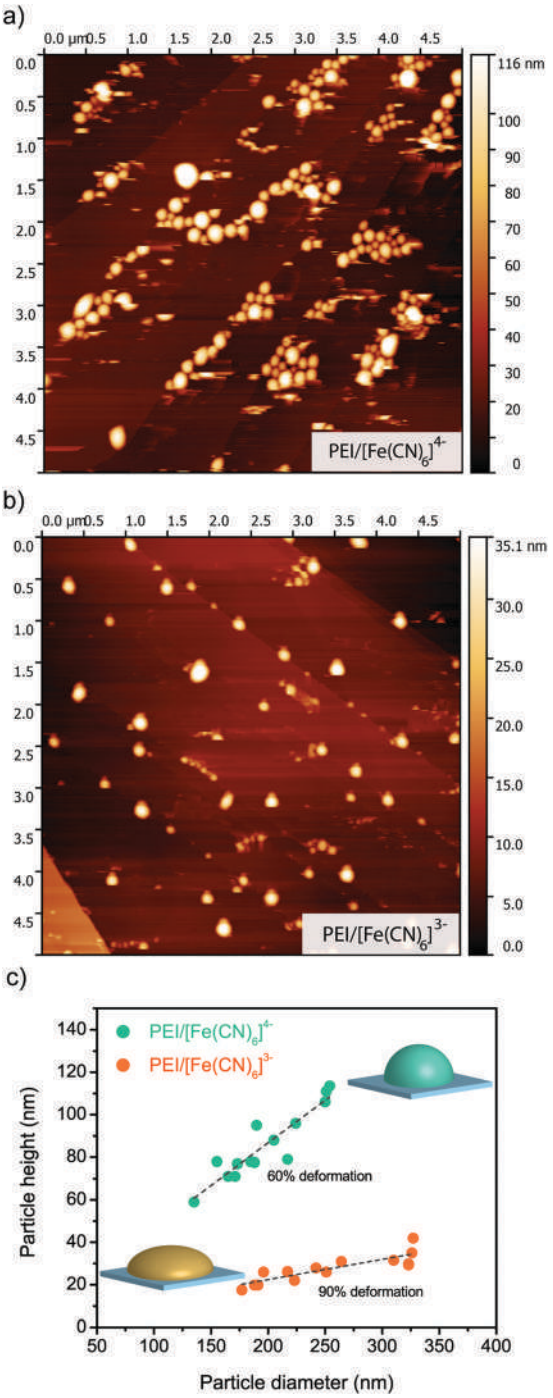

Fig. 1 Contact mode AFM topography images of the Fe(II)-rPSA (a) and Fe(III)-rPSA (b) adsorbed on HOPG. The particle deformation was obtained by plotting height *vs.* diameter and performing a linear regression (c).

contact with the HOPG substrate. Combining this result with the DLS analysis we can argue that when using $[Fe(II)(CN)_6]^{4-}$ as a crosslinker, the rPSA present a more densely packed structure due to the higher capacity of tetravalent anions to form ion pairings with protonated amine groups. As a single iron complex can interact with multiple PEI chains, a contraction effect is produced when increasing the charge of the crosslinker.

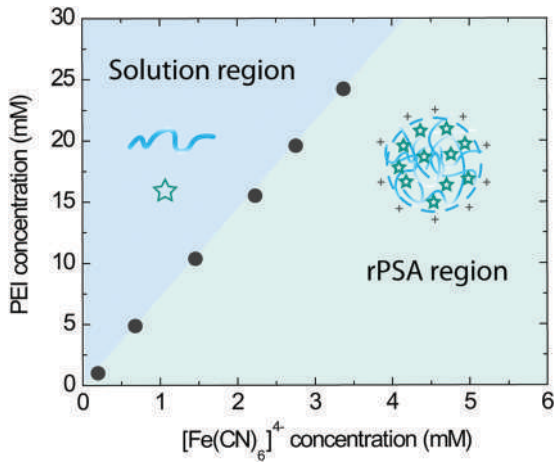

Fig. 2 Phase diagram of Fe(II)-rPSA at pH 3.5 without added salt. On the left side of the curve, the concentration of $[Fe(CN)_6]^{4-}$ is not enough to produce condensation of PEI chains. On the right side of the curve, the system is composed of an rPSA colloidal suspension. The slope of the curve represents the PEI/Fe(II) threshold ratio in order to produce the rPSA colloidal suspension. The *y*-axis denotes the PEI monomer concentration.

rPSA phase diagram analysis

As the main difference between the $[Fe(CN)_6]^{4-}$ and $[Fe(CN)_6]^{3-}$ crosslinkers is the net charge, the molar ratio between PEI and crosslinker at the stage of rPSA formation should differ. To study the effect of the crosslinker charge in the process of rPSA formation, we constructed a phase diagram varying the concentration of PEI and measuring the minimum crosslinker concentration to produce the phase condensation (rPSA formation). Fig. 2 shows the phase diagram for the Fe(II)-rPSA system at pH 3.5 without added salt. The light blue region (solution region) corresponds to a zone of PEI and $[Fe(CN)_6]^{4-}$ concentrations at which the solution is translucent (no rPSA formation). Here, the amount of $[Fe(CN)_6]^{4-}$ is not enough to produce the phase condensation. The light green region (rPSA region) corresponds to a zone of PEI and $[Fe(CN)_6]^{4-}$ concentrations at which the system is a colloidal dispersion of rPSA. The limit between the regions corresponds to the minimum concentration of $[Fe(CN)_6]^{4-}$ to produce rPSA at a given PEI concentration. As there is a linear relation between the PEI and $[Fe(CN)_6]^{4-}$ concentrations, we can attribute the slope of the curve to the maximum molar ratio PEI/Fe(II) necessary to produce phase condensation. In this case, a slope of 7.2 indicates a PEI : Fe(II) of 7 : 1.

Fig. 3a shows the overlaid phase diagrams of the Fe(II)- and Fe(III)-based rPSA at pH 3.5 without added salt. At this pH, the PEI chains are ~90% protonated,[49] so any difference between the systems is attributable to the crosslinkers. Interestingly, the slope of the phase diagram constructed using $[Fe(CN)_6]^{3-}$ (orange dots) is 4.6. Thus, the PEI : Fe(III) molar ratio necessary to produce the phase condensation is about 5 : 1. Comparing this result with the case of PEI:Fe(II), we can argue that for a given concentration of PEI the amount of $[Fe(CN)_6]^{3-}$ necessary to form rPSA is higher than that using $[Fe(CN)_6]^{4-}$. Accordingly, there is a region of PEI and crosslinker concentrations in which rPSA are formed only with $[Fe(CN)_6]^{4-}$. This region is highlighted in red in Fig. 3 and named as the redox region. Inside the redox region, a Fe(II)-rPSA could be selectively disassembled by oxidizing Fe(II) to Fe(III). On the other hand, if the starting point is a translucent solution composed of $[Fe(CN)_6]^{3-}$ and PEI in the redox region, the chemical or electrochemical reduction of Fe(III) to Fe(II) could produce the assembly of the Fe(II)-rPSA. The fact that the slope of the Fe(III)-rPSA phase diagram is lower than the slope of the Fe(II)-rPSA phase diagram can be explained in terms of the charge of the crosslinker. A more

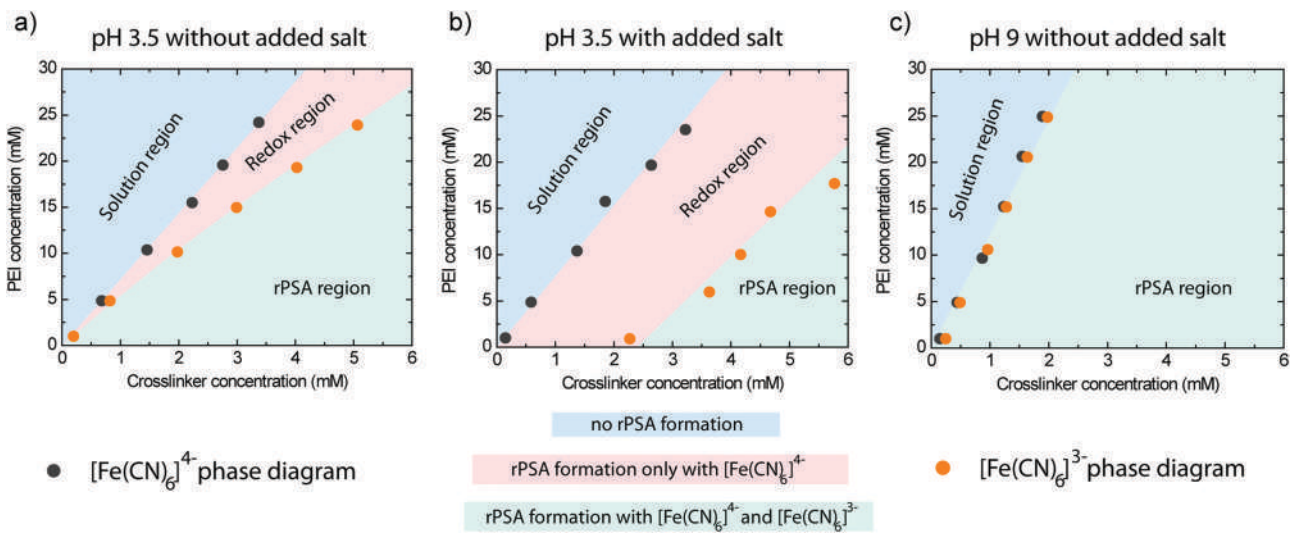

Fig. 3 Overlaid phase diagrams of Fe(II)-rPSA and Fe(III)-rPSA for different conditions: pH 3.5 without added salt (a), pH 3.5 plus 0.2 M NaCl (b), and pH 9 without added salt (c). Curves with black dots correspond to the Fe(II)-rPSA phase diagrams and curves with orange dots correspond to the Fe(III)-rPSA phase diagrams. Different regions are highlighted. In the solution region (light blue), no rPSA are formed. In the redox region (red), rPSA are formed only when $[Fe(CN)_6]^{4-}$ is used as a crosslinker. In the rPSA region (cyan), rPSA are formed with both $[Fe(CN)_6]^{4-}$ and $[Fe(CN)_6]^{3-}$. All experiments were conducted using a 10 kDa PEI polyelectrolyte. The *y*-axis denotes the PEI monomer concentration.

highly charged crosslinker produces the condensation of PEI chains more effectively. It is important to note that similar results were obtained by using a quaternary amine polyelectrolyte like poly(diallyldimethylammonium chloride) (Fig. S2, ESI†). This observation reveals that the formation of a redox region is independent of the nature of the polyamine and that it can be attributed to differences in crosslinking agents. In addition, we also studied the effect of the molecular weight of PEI and found no significant differences between 10 kDa PEI (Fig. 3a) and 750 kDa PEI (Fig. S3, ESI†), indicating that the redox region and phase diagram slopes are independent of the molecular weight of the polyamine.

Outside the redox region, when the concentration of crosslinker is high enough, the stable phase is the colloidal suspension, independently of the crosslinker charge. Under this condition (the rPSA region), both the Fe(II)-rPSA and Fe(III)-rPSA are formed. Thus, the charge of the iron center inside the rPSA can be changed without altering the stability of the colloid. This property opens a path to exploit rPSA as energy storage materials for size-exclusion redox flow batteries.[50–52]

Fig. 3b and c show the overlaid phase diagrams of Fe(II)- and Fe(III)-based rPSA at pH 3.5 with 0.2 M NaCl and at pH 9 without added salt, respectively. Each phase diagram in Fig. 3 was repeated three times in order to demonstrate the reproducibility of these systems (Fig. S4, ESI†). The plots show that (1) the addition of salt at pH 3.5 (most of the amine groups are protonated)[49] amplifies the redox region, shifting the Fe(III)-rPSA phase diagram towards higher concentrations, (2) the slope of both the Fe(II)- and Fe(III)-rPSA phase diagrams increases when the pH is raised to 9 without added salt, and (3) the redox region is lost at pH 9. First, we will discuss the effect of adding NaCl to the system. The slopes of the plots in Fig. 3b are 7.3 and 4.8 for $[Fe(CN)_6]^{4-}$ and $[Fe(CN)_6]^{3-}$, respectively. These values were found to be similar to the case without added salt (7.2 and 4.6, respectively). Thus, the main effect of NaCl addition is to decrease the intercept of the Fe(III)-rPSA phase diagram line, which goes from 0.7 mM to −10 mM (the curve shifts towards higher crosslinker concentrations). Here, an intercept of −10 mM indicates that, even at very small PEI concentrations (lower than 1 mM), the $[Fe(CN)_6]^{3-}$ concentration must be higher than 2 mM to produce the phase condensation. This observation reveals that between 0 and 2 mM $[Fe(CN)_6]^{3-}$ it is not possible to form rPSA. On the other hand, independently of the polymer length, the shift in the intercept by salt addition affects the Fe(III) system but not the Fe(II) system.

When investigating the formation of phosphate-crosslinked poly(allylamine hydrochloride) PSA (PAH/Pi),[19] we demonstrated that a polyamine/crosslinker complex is formed prior to PSA condensation, as evidenced by pH shifting during mixing of reagents. This complexation turns out to be crucial in order to produce the phase condensation. Alternatively, the addition of KCl weakened the polyamine/crosslinker interactions, which resulted in a decrease of the complexation constant and an increase in the ratio Pi/PAH needed to produce PSA. In principle, the differences observed in the Fe(III)-rPSA phase diagrams with and without salt can be explained in terms of competition between Cl^- and $[Fe(CN)_6]^{3-}$ ions for the ammonium groups of PEI, but also by taking into account that increasing the ionic strength lowers the association equilibrium constant of the ionic pairs leading to complexes. Similar observations were reported studying layer-by-layer self-assemblies[37,53,54] and polyelectrolyte brushes[22,55] in the presence of salt ions.

In an attempt to distinguish between these two explanations, we performed phase-diagram studies by adding salts with different anions, while keeping the ionic strength constant. Fig. S5 (ESI†) shows phase diagrams determined in the presence of NaCl, KNO_3 and $LiClO_4$ (anions with different positions in the Hofmeister series). As in the case of NaCl, both KNO_3 and $LiClO_4$ produced a lowering in the intercept of the Fe(III)-rPSA phase diagram which could be explained by screening effects. However, the different phase diagrams observed in the presence of each anion reveal some kind of chemical specificity, which cannot be explained by a simple ionic strength effect. The plot shows that when the anions are more to the right in the Hofmeister series (chaotropic anions), the phase diagram approaches that without added salt. This result is consistent with the hypothesis of specific polyamine–counterion interactions as anions that produce protein salting out, such as Cl^-, tend to form stronger ion pairing with non-quaternary amines. Therefore, a higher proportion of crosslinker $[Fe(CN)_6]^{3-}$ is needed for displacing counterions and inducing phase condensation. In contrast, when using ClO_4^-, the process of anion exchange and crosslinking would be more efficient. These experimental results evidence a complex behavior in which both specific ionic interactions between the polyamine and its counterions and screening effects seem to influence the aggregation behavior of Fe(III)-rPSA in solutions with high salt concentration. On the other hand, regarding the observed difference between the Fe(III) and Fe(II) systems, we believe that the 4 negative charges of the $[Fe(CN)_6]^{4-}$ complex, compared to the 3 negative charges of $[Fe(CN)_6]^{3-}$, allow a complete displacement of amine counterions even at low crosslinker concentrations.

If the phase diagrams in the presence of 0.2 M NaCl are obtained using 750 kDa PEI instead of 10 kDa PEI, the intercept lowers from −10 mM to −3.9 mM (Fig. S6, ESI†). This indicates that the system tends to collapse at a lower $[Fe(CN)_6]^{3-}$ concentration when increasing the chain length. Note that the concentration of PEI is always expressed in terms of monomer concentration in the phase diagrams, so the same concentrations of amine groups are present when comparing experiments performed with 750 kDa and 10 kDa PEI, although the total concentration in terms of polymer chains is different. At low pH (a high degree of protonation), the polyelectrolytes change from an extended conformation at low ionic strength to a coiled conformation in solutions of high ionic strength due to screening of intra-chain electrostatic repulsions.[56,57] In the presence of excess NaCl, $[Fe(CN)_6]^{3-}$ would mainly interact with the fraction of charged amine groups exposed at the surface of the PEI coils. Then, as the fraction of amine groups

exposed to the outside of the coil decreases for increasing molecular weight, the ratio crosslinker/amine needed to induce phase condensation would be lower in the case of 750 kDa PEI. On the contrary, in the absence of added salt, the polyelectrolyte chains would be in extended conformations, so all amine groups would be exposed to the solution and no differences are expected when comparing 10 kDa and 750 kDa PEI phase condensation, as observed in Fig. S3 (ESI†).

When the pH is raised to 9 without added salt, there is a deprotonation of amine groups in PEI. Then, the amount of $-NH_3^+$ groups in PEI is ~22% of the analytical concentration.[49] Under this condition, for a given PEI concentration, less crosslinker is necessary to produce rPSA formation, which explains the increase in the slopes of the phase diagrams. The slopes were found to increase from 7.2 to 13.9 for the Fe(II)-rPSA and from 4.6 to 13.7 for the Fe(III)-rPSA phase diagrams. A similar slope and an intercept around zero indicate a complete loss of the redox region, as can be seen in Fig. 3c.

The variation of the phase diagrams at different conditions of pH, ionic strength and crosslinker identity (Fig. 3) allow inducing either rPSA assembly or disassembly by producing redox reactions and/or moving between regions of the different phase diagrams. Then, the rPSA could be employed as multi-stimuli responsive soft materials as they can be selectively formed and dissolved by altering the pH, ionic strength and redox environment. This idea is not trivial, since although PSA study has grown considerably in recent years, few reports present multitasking platforms with responsiveness to more than one stimulus.[12,14,20] In this framework, the responsive properties of rPSA to the different stimuli are presented and discussed below.

Redox-triggered rPSA assembly/disassembly

The redox-responsiveness of the rPSA system was explored by the addition of oxidizing and reducing agents. Unlike other stimuli, the redox stimulus has been scarcely exploited on colloidal platforms. Historically, electrochemically-active systems have been based on the self-assembly of electroactive polymers with the ability to modulate their properties in response to a redox stimulus.[58,59] In such a framework, the covalent union of ferrocene groups with the polymers was a widely exploited strategy to grant redox-activity to the polymeric building blocks.[60–64] Recently, hexacyanoferrate anions were used as counterions of a quaternary ammonium polyelectrolyte in a chemically synthesized thermo-responsive microgel. The entrapment of electroactive anions generated a material capable of modulating their size by an electrochemical trigger.[34] In our approach, electroactive anions are used directly as crosslinking agents for incorporating redox-responsiveness into the supramolecular nanoarchitecture.

Inside the redox region displayed in Fig. 4a, rPSA can only be formed if $[Fe(CN)_6]^{4-}$ is used as a crosslinking agent. Then, if the iron center is oxidized to Fe(III), the rPSA should be dissolved. On the other hand, if the initial state is a mixture of aqueous solutions of PEI and $[Fe(CN)_6]^{3-}$ (solution phase), the reduction of Fe(III) to Fe(II) should trigger the formation of rPSA.

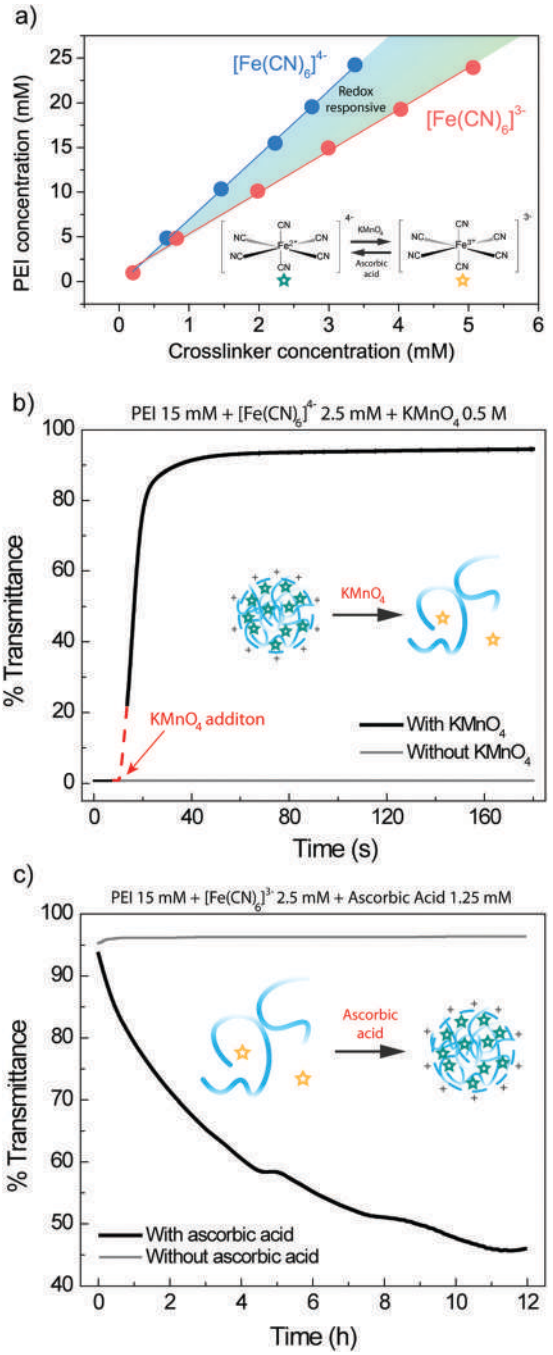

Fig. 4 Redox response. (a) Inside the redox region displayed at the top of the figure (15 mM PEI, 10 kDa and 2.5 mM Fe(II) or Fe(III)), the switching between translucent solution and rPSA colloidal dispersion is achieved by altering the charge of the crosslinker by stoichiometric oxidation with $KMnO_4$ or reduction with ascorbic acid. (b) Fe(II)-rPSA redox-induced disassembly: addition of 0.5 mM $KMnO_4$ into a Fe(II)-rPSA colloidal dispersion (black curve). (c) Fe(II)-rPSA redox-induced assembly: addition of 1.25 mM ascorbic acid into an $[Fe(CN)_6]^{3-}$-containing PEI solution. Grey curves depict blank experiments (without adding redox agents). The turbidity of the solutions was expressed as % transmittance at λ = 580 nm. The red dashed curve represents missing data due to the experimental setup.

Fig. 4a shows a schematic representation of the oxidation of $[Fe(CN)_6]^{4-}$ by treatment with $KMnO_4$ and the reduction of

$[Fe(CN)_6]^{3-}$ by the addition of ascorbic acid. In acid medium, 1 mol of MnO_4^- oxidizes 5 moles of $[Fe(CN)_6]^{4-}$ to give Mn^{2+} (eqn (1)) and 1 mole of ascorbic acid reduces 2 moles of $[Fe(CN)_6]^{3-}$ (eqn (2)).

$$8H^+ + 5[Fe(CN)_6]^{4-} + MnO_4^- \rightarrow 5[Fe(CN)_6]^{3-} + Mn^{2+} + 4H_2O \quad (1)$$

$$C_6H_8O_6 + 2[Fe(CN)_6]^{3-} \rightarrow C_6H_6O_6 + 2[Fe(CN)_6]^{4-} + 2H^+ \quad (2)$$

The redox-triggered disassembly and assembly of Fe(II)-rPSA were conducted at pH 3.5 without added salt using a PEI concentration of 15 mM and a crosslinker concentration of 2.5 mM (see the phase diagrams in Fig. 4a). As the UV-vis spectra of aqueous solutions of $[Fe(CN)_6]^{3-}$, $[Fe(CN)_6]^{4-}$ and PEI do not present appreciable absorbance at λ = 580 nm, changes in the absorbance can be attributed to light scattering. Therefore, we followed the turbidity of the solution by measuring the transmittance percentage (%T) at λ = 580 nm. While a %T near 100% corresponds to a translucent solution (absence of rPSA), a %T near zero corresponds to a cloudy rPSA colloidal dispersion. Fig. 4b shows the dissolution of Fe(II)-rPSA induced by the stoichiometric oxidation of Fe(II) with $KMnO_4$. %T at λ = 580 nm was registered as a function of the time elapsed after the addition of $KMnO_4$. In the experiment, a small aliquot of $KMnO_4$ was injected inside the UV-vis cuvette containing Fe(II)-rPSA and the mixture was vigorously stirred. The red dashed curve in Fig. 4b represents the missing data during this short period of time in which the spectrophotometer was unable to record data. The plot in Fig. 4b shows that Fe(II)-rPSA total dissolution was achieved rapidly, reaching a 90% %T after 25 s of $KMnO_4$ injection. The complete UV-vis spectra of the Fe(II)-rPSA colloidal dispersion before and after the addition of $KMnO_4$ are shown in Fig. S7 (ESI†). From the plot, it can be observed that the final product of the reaction is a translucent solution of $[Fe(CN)_6]^{3-}$. For better comparison, blank spectra of 2.5 mM $[Fe(CN)_6]^{4-}$ and $[Fe(CN)_6]^{3-}$ are also displayed in Fig. S7 (ESI†). As the dissolution of the Fe(II)-rPSA has similar kinetics to the oxidation of $[Fe(CN)_6]^{4-}$ we can say that both processes occur simultaneously, as shown by eqn (3).

$$([Fe(CN)_6]^{4-}/PEI)_{rPSA} + \text{oxidizing agent} \rightarrow [Fe(CN)_6]^{3-} + PEI\ (fast) \quad (3)$$

Fig. 4c shows the formation of Fe(II)-rPSA induced by the stoichiometric reduction of Fe(III) with ascorbic acid. Note the difference in the time scale with Fig. 4b, which indicates that the process is much slower than the dissolution induced by the oxidizing agent. However, the analysis of the UV-visible spectra indicates that the addition of ascorbic acid rapidly reduces the $[Fe(CN)_6]^{3-}$ anions (Fig. S8, ESI†). This indicates that the formation of Fe(II)-rPSA can be described as two sequential processes with distinct kinetics (eqn (4) and (5)): (1) reduction of Fe(III) to Fe(II) (fast) and (2) formation of Fe(II)-rPSA by crosslinking with PEI chains (slow).

$$[Fe(CN)_6]^{3-} + \text{reducing agent} \rightarrow [Fe(CN)_6]^{4-}\ (fast) \quad (4)$$

$$[Fe(CN)_6]^{4-} + PEI \rightarrow ([Fe(CN)_6]^{4-}/PEI)_{rPSA}\ (slow) \quad (5)$$

Thus, the formation of Fe(II)-rPSA by reduction of $[Fe(CN)_6]^{3-}$ anions has slow kinetics with a decrease in %T from 94 to 45% after 12 h. This result opens the following question: why when mixing PEI and $[Fe(CN)_6]^{4-}$ at the same concentrations is rPSA formation a fast process while forming $[Fe(CN)_6]^{4-}$ by $[Fe(CN)_6]^{3-}$ reduction gives a slow rate of rPSA formation? We believe that if the mixing of reagents is conducted using a concentrated solution of crosslinker drop-by-drop, a local increase in the $[Fe(CN)_6]^{4-}$/PEI ratio facilitates the nucleation of the entire colloidal dispersion. On the other hand, if the crosslinker is homogeneously created within the system, as in the case of reducing $[Fe(CN)_6]^{3-}$ anions with ascorbic acid, the nucleation and growth of rPSA occurs in a controlled way. Since Murthy and coworkers elegantly demonstrated a coalescence PSA growth mechanism, the slow aggregation of rPSA could be explained in terms of an initial formation of highly charged colloids that slowly integrate into bigger particles by merging with each other.[39] Further experiments should be conducted in order to determine the differences observed in the nucleation and growth of homogeneously and heterogeneously synthesized PSA.

As the mechanism of rPSA formation may be different according to the experimental procedure, the Fe(II)-rPSA phase diagram constructed by using redox external stimuli may differ from that produced by direct mixing of the reactants. Therefore, to explore the parameter space we prepared different solutions (5 mL) containing PEI (5, 10 and 15 mM) and $[Fe(CN)_6]^{3-}$ at different concentrations and registered their aggregation states (solution or rPSA colloidal dispersion). Then, by addition of 50 μL of ascorbic acid (0.3 M) into each solution, all $[Fe(CN)_6]^{3-}$ complexes were reduced to $[Fe(CN)_6]^{4-}$. After 24 h the aggregation state was registered again. The plots in Fig. S9a and b (ESI†) show the aggregation state before and after the addition of ascorbic acid in comparison with overlaid Fe(II)- and Fe(III)-rPSA phase diagrams obtained by direct mixing. It can be observed that, independently of the procedure, the formation of Fe(II)-rPSA occurs at the same PEI/$[Fe(CN)_6]^{4-}$ ratio. This indicates that the differences found by employing ascorbic acid as an external stimulus are just due to kinetic effects. These results also reinforce the utility of making phase diagrams for guiding the rational understanding and design of stimuli-responsive colloidal systems. Finally, these results suggest that the phase behavior of PSA (solution *vs.* colloidal dispersion) is purely dictated by thermodynamics, while kinetics influences other aspects of the system, such as the particle size and the time evolution of the samples.

pH-triggered rPSA assembly/disassembly

Next, the assembly and disassembly processes in response to pH changes were explored. Fig. 3a shows no rPSA formation when using $[Fe(CN)_6]^{4-}$ as a crosslinker at pH 3.5 without added salt and for concentrations of PEI and $[Fe(CN)_6]^{4-}$ of 20 mM and 2 mM, respectively. Then, if the solution pH is raised to 9 (Fig. 3c), the system switches from the solution region to the rPSA region. Fig. 5a shows overlaid phase diagrams

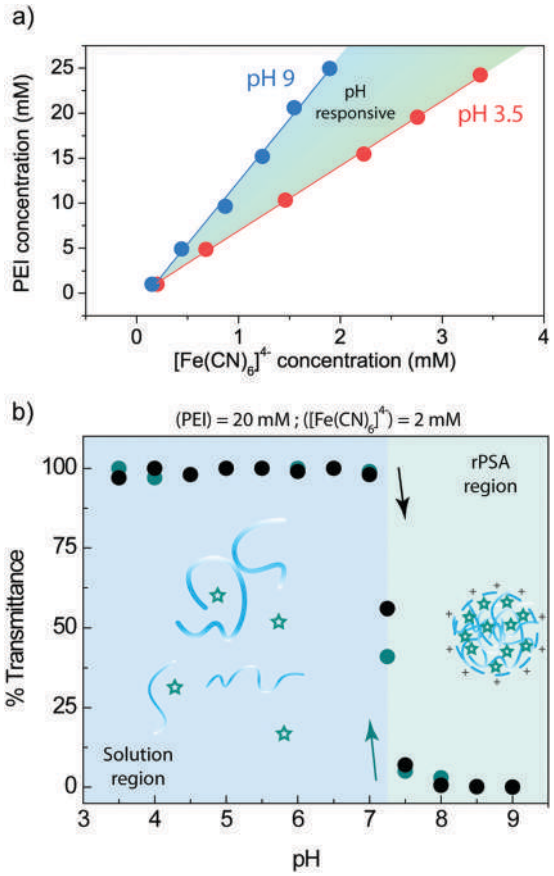

Fig. 5 pH response. (a) Overlaid phase diagrams of Fe(II)-rPSA at pH 3.5 and pH 9. Inside the highlighted zone, the system only forms a colloidal dispersion when pH = 9. (b) A reversible switch between a translucent and a rPSA dispersion is produced by altering the pH from 3.5 to 9 (black dots) and then from 9 to 3.5 (green-blue dots). The initial solution contained 20 mM of PEI (10 kDa) and 2 mM of $[Fe(CN)_6]^{4-}$ without added salt at pH 3.5. The turbidity of the solutions was expressed as %transmittance at λ = 580 nm.

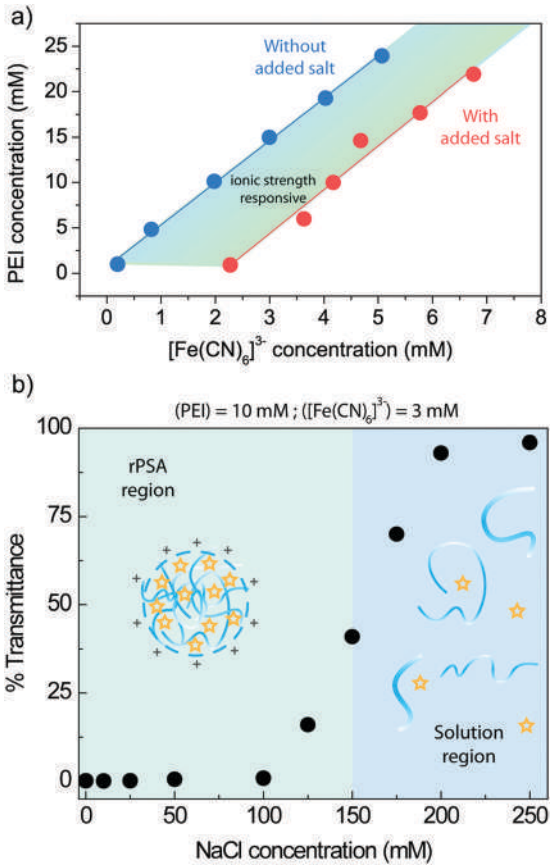

Fig. 6 Ionic strength response. (a) Overlaid phase diagrams of Fe(III)-rPSA at pH 3.5 with and without added salt (0.2 M NaCl). Inside the highlighted zone, the system only forms colloidal dispersion in the absence of added salt. (b) The switch from a rPSA dispersion to a translucent solution is produced by increasing the ionic strength. The initial solution contained 10 mM of PEI (10 kDa) and 3 mM of $[Fe(CN)_6]^{3-}$ without added salt at pH 3.5. The turbidity of the solutions was expressed as %transmittance at λ = 580 nm.

of Fe(II)-rPSA at pH 3.5 and pH 9. Inside the highlighted zone, rPSA are only stable in basic medium, therefore, selective assembly/disassembly of rPSA could be achieved by changing the solution pH. The black dots in Fig. 5b show the evolution of $\%T$ when the pH is raised from 3.5 to 9. As can be observed in the plot, when the solution pH is higher than 7, an abrupt decrease in $\%T$ is detected, which indicates the pH-triggered formation of rPSA. The green-blue dots in Fig. 5 show the evolution of $\%T$ when the pH is lowered from 9 to 3.5. In this case, when the pH is lower than 7.5, $\%T$ increases dramatically, indicating pH-triggered rPSA disassembly. In the same way, if now $[Fe(CN)_6]^{3-}$ is used as a crosslinking agent, similar behavior is observed (see Fig. S10 in the ESI†). These results show that both Fe(II)- and Fe(III)-rPSA could be exploited as reversible pH-sensitive soft nanoparticles.

Salt-induced rPSA disassembly

Finally, the ionic strength responsiveness was evaluated for Fe(III)-rPSA. A rPSA colloidal dispersion is observed when using $[Fe(CN)_6]^{3-}$ as a crosslinking agent at pH 3.5 without added salt and for concentrations of PEI and $[Fe(CN)_6]^{3-}$ of 10 mM and 3 mM, respectively (see the rPSA region in Fig. 3a). Then, if NaCl is added into the system until reaching a concentration of 0.2 M the solution phase becomes the stable phase (Fig. 3b). Fig. 6a shows overlaid phase diagrams of Fe(III)-rPSA at pH 3.5 with and without the addition of 0.2 M NaCl. Inside the highlighted zone the rPSA colloidal dispersion is only stable in the absence of added salt; therefore, rPSA could be selectively dissolved by increasing the medium ionic strength. Fig. 6b shows the variation of $\%T$ for increasing NaCl concentration. The plot shows that between 0 and 100 mM the solution remains fully cloudy. Above this value, there is a linear increase in $\%T$ until reaching a maximum and constant value, indicating the complete dissolution of the colloidal dispersion. In this way, Fe(III)-rPSA could be employed as ionic strength-sensitive soft nanoparticles.

Conclusions

In this work we used $[Fe(CN)_6]^{4-}$ and $[Fe(CN)_6]^{3-}$ anions as redox-active crosslinking agents for the one-pot formation of

PEI-based rPSA. By constructing phase diagrams, varying the concentration of each building block under different experimental conditions, we determined three distinct regions: the solution region, redox region and rPSA region. These three regions enabled the multi-stimuli response of the system. Under specific PEI and crosslinker concentrations, we showed that shifting the solution pH produced the reversible assembly/disassembly of both Fe(II)- and Fe(III)-rPSA. Also, we proved that Fe(III)-rPSA can be selectively dissolved by the addition of salt.

More interestingly, as the charge of the crosslinker is a key factor in the formation and stability of PSA colloidal dispersions, we have demonstrated that inside the redox region rPSA can only be formed when $[Fe(CN)_6]^{4-}$ anions are used as crosslinking agents. Under this condition, we showed that (1) the addition of an oxidizing agent produced the dissolution of Fe(II)-rPSA, and (2) the addition of a reducing agent produced the formation of Fe(II)-rPSA. Notoriously, while the disassembly of rPSA turned out to be a fast process, the assembly had slow kinetics. Considering that PSA are used as nanocarriers for drug delivery and controlled release, the slow assembly of Fe(II)-rPSA could be applied for controlled entrapment of key small molecules under reducing conditions. On the other hand, this controllable assembly kinetics could be rationally exploited for the electrochemical buildup of electroactive films.

In summary, we believe that the possibility of modulating the assembly and disassembly of the system by applying different stimuli offers opportunities and possible applications in nanotechnology, including electro-triggered actuators, controlled release devices, and electroactive functional films, among others.

Conflicts of interest

There are no conflicts to declare.

Acknowledgements

This work was supported by the Consejo Nacional de Investigaciones Científicas y Técnicas (CONICET, Argentina) (Grant No. PIP 0370), Agencia Nacional de Promoción Científica y Tecnológica (ANPCyT, Argentina; PICT-2016-1680, PICT-2017-1523), the Austrian Institute of Technology GmbH (AIT-CONICET Partner Group: ''Exploratory Research for Advanced Technologies in Supramolecular Materials Science'', Exp. 4947/11, Res. No. 3911, 28-12-2011), and Universidad Nacional de La Plata (UNLP). M. L. C., W. A. M., M. T. and O. A. are staff members of CONICET. M. L. A. and S. E. H. gratefully acknowledge CONICET for their postdoctoral fellowships.

References

1 H. S. El-Sawy, A. M. Al-Abd, T. A. Ahmed, K. M. El-Say and V. P. Torchilin, *ACS Nano*, 2018, **12**, 10636–10664.
2 Y. Zhou, H. Ye, Y. Chen, R. Zhu and L. Yin, *Biomacromolecules*, 2018, **19**, 1840–1857.
3 J. Zhao, V. E. Lee, R. Liu and R. D. Priestley, *Annu. Rev. Chem. Biomol. Eng.*, 2019, **10**, 361–382.
4 Z.-Q. Cao and G.-J. Wang, *Chem. Rec.*, 2016, **16**, 1398–1435.
5 X. Fu, L. Hosta-Rigau, R. Chandrawati and J. Cui, *Chem*, 2018, **4**, 2084–2107.
6 P. Schattling, F. D. Jochum and P. Theato, *Polym. Chem.*, 2014, **5**, 25–36.
7 S. Guragain, B. P. Bastakoti, V. Malgras, K. Nakashima and Y. Yamauchi, *Chem. – Eur. J.*, 2015, **21**, 13164–13174.
8 R. Cheng, F. Meng, C. Deng, H.-A. Klok and Z. Zhong, *Biomaterials*, 2013, **34**, 3647–3657.
9 G. Pasparakis and M. Vamvakaki, *Polym. Chem.*, 2011, **2**, 1234.
10 F. D. Jochum and P. Theato, *Chem. Soc. Rev.*, 2013, **42**, 7468–7483.
11 Y. Dong, J. Wang, X. Guo, S. Yang, M. O. Ozen, P. Chen, X. Liu, W. Du, F. Xiao, U. Demirci and B.-F. Liu, *Nat. Commun.*, 2019, **10**, 4087.
12 H. G. Bagaria and M. S. Wong, *J. Mater. Chem.*, 2011, **21**, 9454–9466.
13 R. K. Rana, V. S. Murthy, J. Yu and M. S. Wong, *Adv. Mater.*, 2005, **17**, 1145–1150.
14 Y. Lapitsky, *Curr. Opin. Colloid Interface Sci.*, 2014, **19**, 122–130.
15 J. Yu, D. Javier, M. A. Yaseen, N. Nitin, R. Richards-Kortum, B. Anvari and M. S. Wong, *J. Am. Chem. Soc.*, 2010, **132**, 1929–1938.
16 M. L. Agazzi, S. E. Herrera, M. L. Cortez, W. A. Marmisollé, C. von Bilderling, L. I. Pietrasanta and O. Azzaroni, *Soft Matter*, 2019, **15**, 1640–1650.
17 W. A. Marmisollé, J. Irigoyen, D. Gregurec, S. Moya and O. Azzaroni, *Adv. Funct. Mater.*, 2015, **25**, 4144–4152.
18 P. Andreozzi, E. Diamanti, K. R. Py-Daniel, P. R. Cáceres-Vélez, C. Martinelli, N. Politakos, A. Escobar, M. Muzi-Falconi, R. Azevedo and S. E. Moya, *ACS Appl. Mater. Interfaces*, 2017, **9**, 38242–38254.
19 S. E. Herrera, M. L. Agazzi, M. L. Cortez, W. A. Marmisollé, M. Tagliazucchi and O. Azzaroni, *ChemPhysChem*, 2019, **20**, 1044–1053.
20 S. E. Herrera, M. L. Agazzi, M. L. Cortez, W. A. Marmisollé, M. Tagliazucchi and O. Azzaroni, *Chem. Commun.*, 2019, **55**, 14653–14656.
21 M. A. Frías, G. Contis, A. Hollmann and E. A. Disalvo, *Colloids Surf., B*, 2012, **91**, 26–33.
22 E.-Y. Choi, O. Azzaroni, N. Cheng, F. Zhou, T. Kelby and W. T. S. Huck, *Langmuir*, 2007, **23**, 10389–10394.
23 V. S. Vasantha and S.-M. Chen, *Electrochim. Acta*, 2005, **51**, 347–355.
24 E. Spruijt, E.-Y. Choi and W. T. S. Huck, *Langmuir*, 2008, **24**, 11253–11260.
25 X. Zhuang, D. Wang, Y. Lin, L. Yang, P. Yu, W. Jiang and L. Mao, *Anal. Chem.*, 2012, **84**, 1900–1906.
26 C. Qin, W. Wang, C. Chen, L. Bu, T. Wang, X. Su, Q. Xie and S. Yao, *Sens. Actuators, B*, 2013, **181**, 375–381.
27 O. Mergel, A. P. H. Gelissen, P. Wünnemann, A. Böker, U. Simon and F. A. Plamper, *J. Phys. Chem. C*, 2014, **118**, 26199–26211.

28 M. V. Martinez, M. M. Bruno, M. C. Miras and C. A. Barbero, *Electrochim. Acta*, 2016, **219**, 363–376.
29 T. A. García, C. A. Gervasi, M. J. Rodríguez Presa, J. I. Otamendi, S. E. Moya and O. Azzaroni, *J. Phys. Chem. C*, 2012, **116**, 13944–13953.
30 M. Ohyanagi and F. C. Anson, *J. Electroanal. Chem. Interfacial Electrochem.*, 1989, **258**, 469–477.
31 M. Ohyanagi and F. C. Anson, *J. Phys. Chem.*, 1989, **93**, 8377–8382.
32 O. Mergel, P. T. Kühn, S. Schneider, U. Simon and F. A. Plamper, *Electrochim. Acta*, 2017, **232**, 98–105.
33 F. A. Plamper, L. Murtomäki, A. Walther, K. Kontturi and H. Tenhu, *Macromolecules*, 2009, **42**, 7254–7257.
34 O. Mergel, P. Wünnemann, U. Simon, A. Böker and F. A. Plamper, *Chem. Mater.*, 2015, **27**, 7306–7312.
35 J. Liang, M. C. Elliot and V. Cammarata, *Electroanalysis*, 2009, **21**, 2542–2548.
36 B. Wang and J. I. Anzai, *Langmuir*, 2007, **23**, 7378–7384.
37 D. Grieshaber, J. Vörös, T. Zambelli, V. Ball, P. Schaaf, J.-C. Voegel and F. Boulmedais, *Langmuir*, 2008, **24**, 13668–13676.
38 S. Schneider, C. Janssen, E. Klindtworth, O. Mergel, M. Möller and F. Plamper, *Polymers*, 2018, **10**, 429.
39 V. S. Murthy, R. K. Rana and M. S. Wong, *J. Phys. Chem. B*, 2006, **110**, 25619–25627.
40 P. G. Lawrence and Y. Lapitsky, *Langmuir*, 2015, **31**, 1564–1574.
41 G. Agrawal and R. Agrawal, *Small*, 2018, **14**, 1801724.
42 K. H. Tan, W. Xu, S. Stefka, D. E. Demco, T. Kharandiuk, V. Ivasiv, R. Nebesnyi, V. S. Petrovskii, I. I. Potemkin and A. Pich, *Angew. Chem., Int. Ed.*, 2019, **58**, 9791–9796.
43 R. Contreras-Cáceres, J. Pacifico, I. Pastoriza-Santos, J. Pérez-Juste, A. Fernández-Barbero and L. M. Liz-Marzán, *Adv. Funct. Mater.*, 2009, **19**, 3070–3076.
44 G. Agrawal and R. Agrawal, *Polymers*, 2018, **10**, 418.
45 S. Wellert, Y. Hertle, M. Richter, M. Medebach, D. Magerl, W. Wang, B. Demé, A. Radulescu, P. Müller-Buschbaum, T. Hellweg and R. von Klitzing, *Langmuir*, 2014, **30**, 7168–7176.
46 A. Mourran, Y. Wu, R. A. Gumerov, A. A. Rudov, I. I. Potemkin, A. Pich and M. Möller, *Langmuir*, 2016, **32**, 723–730.
47 V. E. Cuenca, H. Martinelli, M. de los, A. Ramirez, H. A. Ritacco, P. Andreozzi and S. E. Moya, *Langmuir*, 2019, **35**, 14300–14309.
48 S. E. Herrera, M. L. Agazzi, M. L. Cortez, W. A. Marmisollé, C. Bilderling and O. Azzaroni, *Macromol. Chem. Phys.*, 2019, 1900094.
49 H. J. Kong and D. J. Mooney, *Cell Transplant.*, 2003, **12**, 779–785.
50 X. Ke, J. M. Prahl, J. I. D. Alexander, J. S. Wainright, T. A. Zawodzinski and R. F. Savinell, *Chem. Soc. Rev.*, 2018, **47**, 8721–8743.
51 E. C. Montoto, G. Nagarjuna, J. Hui, M. Burgess, N. M. Sekerak, K. Hernández-Burgos, T.-S. Wei, M. Kneer, J. Grolman, K. J. Cheng, J. A. Lewis, J. S. Moore and J. Rodríguez-López, *J. Am. Chem. Soc.*, 2016, **138**, 13230–13237.
52 Z. T. Gossage, K. Hernández-Burgos, J. S. Moore and J. Rodríguez-López, *ChemElectroChem*, 2018, **5**, 3006–3013.
53 J. Irigoyen, S. E. Moya, J. J. Iturri, I. Llarena, O. Azzaroni and E. Donath, *Langmuir*, 2009, **25**, 3374–3380.
54 O. Azzaroni, S. E. Moya, A. A. Brown, Z. Zheng, E. Donath and W. T. S. Huck, *Adv. Funct. Mater.*, 2006, **16**, 1037–1042.
55 O. Azzaroni, S. Moya, T. Farhan, A. A. Brown and W. T. S. Huck, *Macromolecules*, 2005, **38**, 10192–10199.
56 K. A. Curtis, D. Miller, P. Millard, S. Basu, F. Horkay and P. L. Chandran, *PLoS One*, 2016, **11**, e0158147.
57 S. Moya, O. Azzaroni, T. Farhan, V. L. Osborne and W. T. S. Huck, *Angew. Chem., Int. Ed.*, 2005, **44**, 4578–4581.
58 J. P. Cook and D. J. Riley, *J. Polym. Sci., Part B: Polym. Phys.*, 2012, **50**, 516–522.
59 D. Chong, J. Tan, J. Zhang, Y. Zhou, X. Wan and J. Zhang, *Chem. Commun.*, 2018, **54**, 7838–7841.
60 Y. Ma, W.-F. Dong, M. A. Hempenius, H. Möhwald and G. Julius Vancso, *Nat. Mater.*, 2006, **5**, 724–729.
61 X. Sui, M. A. Hempenius and G. J. Vancso, *J. Am. Chem. Soc.*, 2012, **134**, 4023–4025.
62 Z. Wang, H. Möhwald and C. Gao, *Langmuir*, 2011, **27**, 1286–1291.
63 O. Mergel, S. Schneider, R. Tiwari, P. T. Kühn, D. Keskin, M. C. A. Stuart, S. Schöttner, M. de Kanter, M. Noyong, T. Caumanns, J. Mayer, C. Janzen, U. Simon, M. Gallei, D. Wöll, P. van Rijn and F. A. Plamper, *Chem. Sci.*, 2019, **10**, 1844–1856.
64 L. Peng, A. Feng, M. Huo and J. Yuan, *Chem. Commun.*, 2014, **50**, 13005–13014.

